# Removal of hexavalent chromium using durian in the form of rind, cellulose, and activated carbon: Comparison on adsorption performance and economic evaluation

Carlos David Sulistiyo [a,1], Kuan-Chen Cheng [b,c,d,e,1], Henoch Jaya Su'andi [a,1], Maria Yuliana [a,f], Chang-Wei Hsieh [g,h], Suryadi Ismadji [a,f], Artik Elisa Angkawijaya [i,***], Alchris Woo Go [j], Hsien Yi Hsu [k,l,**], Phuong Lan Tran-Nguyen [m], Shella Permatasari Santoso [a,f,*]

[a] Chemical Engineering Department, Faculty of Engineering, Widya Mandala Surabaya Catholic University, Surabaya, 60114, East Java, Indonesia
[b] Institute of Food Science and Technology, National Taiwan University, No. 1, Sec. 4, Roosevelt Road, Taipei, 10617, Taiwan
[c] Institute of Biotechnology, National Taiwan University, No. 1, Sec. 4, Roosevelt Road, Taipei, 10617, Taiwan
[d] Department of Medical Research, China Medical University Hospital, Taichung, 40402, Taiwan
[e] Department of Optometry, Asia University, 500, Lioufeng Road, Wufeng, Taichung, 41354, Taiwan
[f] Collaborative Research Center for Zero Waste and Sustainability, Jl. Kalijudan 37, Surabaya, 60114, East Java, Indonesia
[g] Department of Food Science and Biotechnology, National Chung Hsing University, South Dist., Taichung City, 40227, Taiwan
[h] Department of Medical Research, China Medical University Hospital, North Dist., Taichung City, 404333, Taiwan
[i] Center for Sustainable Resource Science, RIKEN, Yokohama, Japan
[j] Department of Chemistry, National Taiwan University of Science and Technology, Taipei, 10607, Taiwan
[k] School of Energy and Environment, Department of Materials Science and Engineering, City University of Hong Kong, Kowloon Tong, Hong Kong, China
[l] Shenzhen Research Institute of City University of Hong Kong, Shenzhen, 518057, China
[m] Department of Mechanical Engineering, Can Tho University, Campus II, 3/2 Street, Can Tho City, 900100, Viet Nam

## ARTICLE INFO

## ABSTRACT

Durian rind (DR) is one of the lignocellulose-containing agro-industrial wastes abundant in many South Asian counties. Contributing toward a sustainable and zero waste future, DR was utilized as raw material for cellulose and activated carbon production. A chemical delignification method was adopted to valorize DR into cellulose, while carbonization and subsequent KOH activation steps were used to convert the DR into activated carbon. The resulting materials exhibited high adsorption capacity toward $Cr^{6+}$ (154.2 and 223.3 mg/g for cellulose and activated carbon, respectively). The activated carbon derived from DR exhibited a faster adsorption rate of $Cr^{6+}$ compared to cellulose and raw DR. The adsorption of $Cr^{6+}$ by DR-derived adsorbents exhibited a monolayer tendency, with isotherm and kinetics data following the Khan and pseudo-second-order models. The total production cost of converting DR into cellulose and activated carbon was evaluated using life-cycle cost analysis (LCCA). Compared to the cellulose production, DR to activated carbon conversion requires up to 6-fold higher cost for energy. Based on the economic analysis, ~US$ 2.9 and US$ 4.2 were needed to convert 1 kg DR into cellulose and activated carbon, respectively.

* Corresponding author. Chemical Engineering Department, Faculty of Engineering, Widya Mandala Surabaya Catholic University, Surabaya, 60114, East Java, Indonesia.
** Corresponding author. School of Energy and Environment, Department of Materials Science and Engineering, City University of Hong Kong, Kowloon Tong, Hong Kong, China.
*** Corresponding author. Center for Sustainable Resource Science, RIKEN, Yokohama, Japan.
*E-mail addresses:* artikelisa.angkawijaya@riken.jp (A.E. Angkawijaya), sam.hyhsu@cityu.edu.hk (H.Y. Hsu), shella_p5@yahoo.com, shella@ukwms.ac.id (S.P. Santoso).
[1] These authors are contributed equally to this work.

## 1. Introduction

In the past decades, various efforts have been made to actualize waste reduction and achieve a zero-waste future. One of them is through the valorization of biomass waste thus minimize their accumulation in landfill (Chintagunta et al., 2021; Davies et al., 2021; Offei et al., 2021). Lignocellulose-containing biomass (LCB) from agro-industrial residues is one of the most abundant biomass waste in Southeast Asian countries like Indonesia. Some forms of LCB are sugarcane bagasse, rice husks, corn cobs, and durian rind (DR), among others, with the latter being the main focus of this work. Indonesia is listed among the major durian-producing countries along with Malaysia, Thailand, and Vietnam, which translates to opportunities for valorizing and utilizing DR as a renewable resource. In an annual report by Statistic Indonesia (Fig. 1a), durian plantation is available in almost all provinces in Indonesia, with Java having the highest production capacity at $447 \pm 19$ metric tons (MT) annually. Additionally, because of the increasing demand for durian, in 2017, the Indonesian government opened another 5000 ha of durian plantations (Bisara and Muchtar, 2018), which resulted in a drastic increase in durian production in 2018. The support from the government accommodates the increase in the export of processed durian fruits (Fig. 1b), which consequently increases the generation of its residues in the form of DR. Constituting 75–80% of the total fruit weight, DR at an average of $764 \pm 17$ MT annually could be generated, considering that the total durian production is 735–1374 MT from 2012 to 2021 (Fig. 1c). Given the large quantities of DR, its size, volume, and morphology, it poses disposal issues and can negatively impact the environment if not addressed. Thus, this work intended to explore the potential of DR as raw material for production of value-added materials.

The conversion of waste into high-value-added products can be a potential economic strategy to reduce waste accumulation, maximize resource utilization, and develop a more competitive economy (Osman et al., 2020a). In this work, the sustainable features of DR are further explored. As a residue that is generated annually at a stable and increasing rate, DR is currently underutilized, but its renewable nature makes it a potential candidate as a sustainable resource. Carbon content in DR is high and is primarily from its constituent lignocellulosic components, 61% cellulose, 13% hemicellulose, and ~23% lignin (Tan et al., 2017). Thus, it is expected that value-added materials, like cellulose (DR-Cel) and activated carbon (DR-AC), could be derived from DR to serve as bio-adsorbents. To evaluate their applicability, the materials derived from DR were utilized as an adsorbent for removing the toxic hexavalent chromium ($Cr^{6+}$) (Abreu et al., 2018). The direct use of DR as an adsorbent for heavy metal removal has been reported before (Ngabura et al., 2018). Despite its adsorption potential, untreated DR is prone to wilts and spoils during transport and storage due to high glucan and xylan content (Obeng et al., 2018). Thus, a suitable valorization procedure is needed for efficient waste-to-product conversion and addressing the spoilage issue.

Various techniques can be implemented to reduce or eliminate $Cr^{6+}$ from water and wastewater, including ion exchange, membrane separation, precipitation, electrolysis, adsorption, etc. Among them, adsorption is the simplest and the lowest cost; this technique involves the direct addition of adsorbents into polluted water without requiring complex equipment and chemical additives. Meanwhile, the associated cost of initial equipment setup and/or requirements of auxiliary chemicals makes other treatments less economically appealing (Peng and Guo, 2020). Although adsorption is favored for its ease of operation and lower operational costs, the cost and non-renewability of synthetic adsorbents have raised some concerns, particularly in term of its sustainability. To cope with this issue, several low-cost adsorbents from renewable materials were developed (Islam et al., 2019). In this context, locally available LCB residue, particularly DR, were deemed as the proper raw material applicable for the wastewater treatment. Additionally, it would serve as a new industry which create economic gains and play part in environment preservation. Furthermore, although DR can be a promising inexpensive LCB, the method and chemicals used to



a) Production of durian fruit per province in Indonesia from 2015 to 2019

b) Total import of durian fruit

c) Total production of fruit vs rind
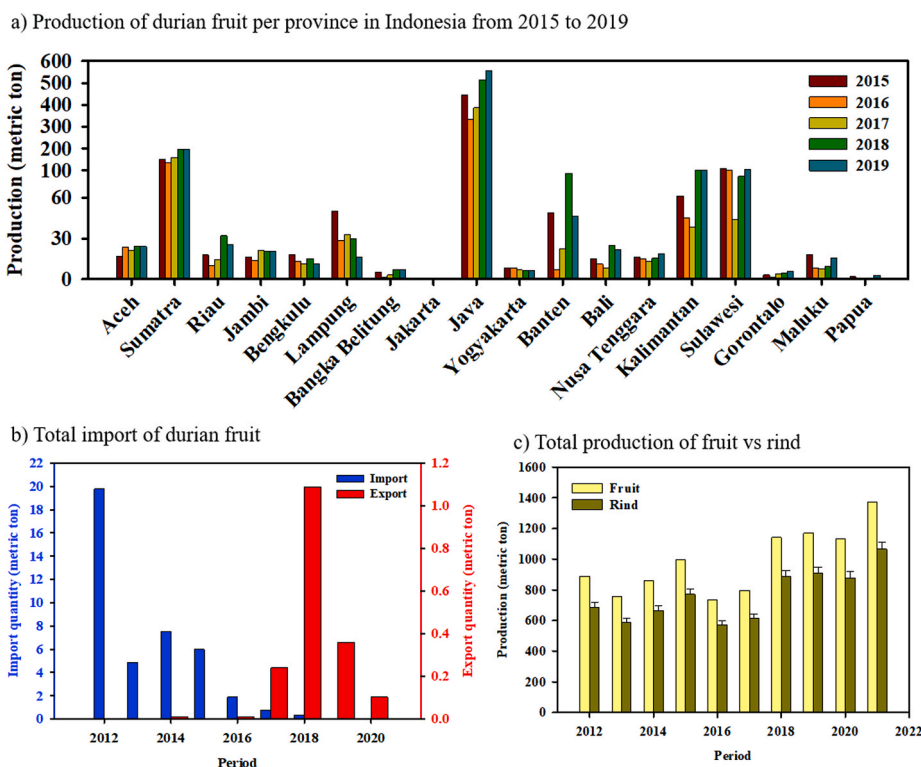
**Fig. 1.** **a)** Production of durian fruit from each province in Indonesia from 2015 to 2019, reported by Statistics Indonesia. **b)** Import and export data of durian in Indonesia from 2012 to 2020; data were retrieved from UN Comtrade (https://comtrade.un.org/data/). **c)** Total production of durian fruit (https://www.pertanian.go.id) and the estimated rind generation based on annual durian fruit production.

produce the product may become the pivotal challenge in establishing a cost-effective approach. Herein, we demonstrated a straightforward economic analysis to estimate the total production cost through life-cycle cost analysis (LCCA), which can be an essential reference for evaluating the economic feasibility of a process (Wang et al., 2021). To the best of our knowledge, this work is the first to detail the $Cr^{6+}$-adsorption performance and production cost analysis of DR to DR-based adsorbents conversion.

## 2. Materials and method

### 2.1. Materials

Durian rind (DR) was collected from the local market in Surabaya, East Java, Indonesia; the durian was a Monthong Bali variety. The collected DR was directly rinsed with water, cut into small pieces, and dried in an oven at 70 °C for three days. An ACS reagent 1,5-diphenyl-carbazide ($C_{13}H_{14}N_4O$), potassium hydroxide (KOH, 90% purity), sulfuric acid ($H_2SO_4$, 97% purity), and acetone ($CH_3COCH_3$, 99.5%) were obtained from Merck, Germany. Sodium chlorite 12% ($NaClO_2$), acetic acid ($CH_3COOH$, 98% purity), ethanol ($C_2H_5OH$, 97% purity), $FeCl_3 \cdot 6H_2O$ (99% purity), and $K_2Cr_2O_7$ (99.5% purity) was purchased from SAP Chemical, Indonesia. The chemicals were used directly without further purification.

### 2.2. Conversion of DR into cellulose (DR-Cell)

Dried DR (40 g) was soaked in water at a mass-to-volume ratio of 1:10 for 24 h at room temperature, then DR was reduced in size and pulped using a blender. Acetic acid (1 mL) and $NaClO_2$ (2 mL) were then added to 100 mL DR pulp every 1 h for a total duration of 5 h —This step was used to weaken the lignin bonds and promote their dissolution (Gill et al., 2021). The DR pulp was thoroughly rinsed with tap water until the yellow color disappeared, and after that, pressed to remove as much water as possible. The bleached DR pulp was soaked in 80 mL of 17.5% (w/v) NaOH solution for 1 h, 5 mL of NaOH solution at the same concentration was added at an interval of 15 min for three times. The pretreated pulp was collected and soaked in 200 mL of 8.3% (w/v) NaOH solution for 15 min. Then, the pulp was collected and soaked in 200 mL of 10% acetic acid for 15 min to neutralize the excess NaOH and accelerate the next washing step. The obtained solid was washed with a conspicuous amount of water to remove the excess chemicals and was dried in an oven at 80 °C for two days to collect the DR-Cel. The final cellulose content was $79.92 \pm 2.18\%$ from $37.68 \pm 0.04\%$ initially.

### 2.3. Conversion of DR into activated carbon (DR-AC)

DR was soaked in water at a mass-to-volume ratio of 1:30 for 24 h at room temperature. After soaking to soften the fibers, DR was pulped using a blender. The resulting pulp was then dried in an oven at 80 °C for two days. The activated carbon was produced following the reported procedure by Ahmed et al. (2019) with slight modification. Briefly, the dried DR pulp was placed in a covered crucible and carbonized in a furnace at 500 °C for 2 h. The obtained chars were crushed, and the powder was sieved to collect particles with the size of +60/-80 mesh. The fine carbonized DR powder was impregnated with KOH, at a KOH-to-carbon weight ratio of 4:1. Activation was carried out in a furnace at 500 °C for 1 h to obtain the activated carbon DR-AC.

### 2.4. Surface characterization and textural properties

Surface morphology analysis was performed using the scanning electron microscopy (SEM) method using a JEOL JSM-7900F field emission SEM. Before analysis, the samples were coated with a Pd/Pt film using JEOL JEC3000FC fine coater. Crystallinity pattern analysis was done by applying X-ray diffraction (XRD) analysis using a Bruker D2

Phaser X-ray diffractometer. The functional group composition was characterized by utilizing Fourier transform infrared (FTIR) spectroscopy using a Bio-Rad FTS-3500GX FTIR spectrophotometer; KBr was used as the background spectra. The porosity of the samples was measured using $N_2$ sorption isotherm analysis using a Quadrasorb SI analyzer.

### 2.5. Adsorption studies

Adsorption studies were carried out to remove $Cr^{6+}$; the initial and residual concentration of $Cr^{6+}$ was determined by employing colorimetric using a 1,5-diphenylcarbazide reagent; the detailed procedure can be found elsewhere (Lace et al., 2019). The adsorption study was divided into three parts as follows:

(1) *Study of the effect of* pH: A stock solution of $Cr^{6+}$ at a concentration of 2500 mg/L was prepared by dissolving $K_2Cr_2O_7$ into water. Then, a series of 50 mL $Cr^{6+}$ solutions at 250 mg/L was prepared by diluting the stock solution. The pH of the solution was adjusted from 2 to 10; then, 0.2g of adsorbent was introduced, and the adsorption process was carried out for 8 h.
(2) *Adsorption isotherm*: A series of $Cr^{6+}$ solutions at different concentrations were prepared by diluting the stock solution. Then, 0.2g of adsorbent was added to each flask. The adsorption was run for 8 h, and the residual concentration of $Cr^{6+}$ was determined using the colorimetric procedure.
(3) *Adsorption kinetic*: A series of $Cr^{6+}$ solutions at 250 mg/L was prepared by diluting the stock solution. Then, 0.2g of adsorbent was added to each flask. The residual concentration of $Cr^{6+}$ was determined using the colorimetric procedure at a predetermined time.

### 2.6. Adsorption analysis

The final concentration of $Cr^{6+}$ in the bulk solution after adsorption is expressed as $C_e$ (mg/L). The amount of $Cr^{6+}$ adsorbed by the adsorbent is defined as $Q_e$ (mg/g), calculated by equation (1).

$$Q_e = \frac{(C_0 - C_e)}{m} \times V \tag{1}$$

where $C_0$ is the initial $Cr^{6+}$ concentration (mg/L), $V$ is the total volume (L), and $m$ is adsorbent mass (g).

The pseudo-1st-order (P1O), pseudo-2nd-order (P2O), Elovich, and intraparticle diffusion (IPD) models were used in describing the kinetic data (Revellame et al., 2020). The mathematical expression of P1O is given in equation (2).

$$Q_t = Q_1 \left(1 - e^{-k_1 t}\right) \tag{2}$$

Here, $Q_1$ is the adsorption capacity (mg/g), and $k_1$ is the rate constant (1/min).

The P2O model can be mathematically expressed as equation (3).

$$Q_t = Q_2 \frac{k_2 Q_2 t}{1 + k_2 Q_2 t} \tag{3}$$

where $Q_2$ is the adsorption capacity (mg/g), and $k_2$ is the rate constant (g/mg min).

The dimensionless Elovich equation is mathematically expressed as equation (4).

$$\frac{Q_t}{Q_{ref}} = R_E \ln \frac{t}{t_{ref}} + 1 \tag{4}$$

where $Q_{ref}$ is the measured adsorption capacity (mg/g) at $t_{ref}$, with $t_{ref}$ being the longest time in the adsorption system. $R_E$ is the dimensionless equilibrium constant.

The non-linear IPD model can be carried out by applying equation (5).

$$\frac{Q_t}{Q_{\text{ref}}} = 1 - R_{\text{IPD}} \left[ 1 - \left( \frac{t}{t_{\text{ref}}} \right)^{1/2} \right] \tag{5}$$

where $R_{\text{IPD}}$ is an initial adsorption factor.

Four adsorption isotherm models were tested in describing and understanding the distribution of $Cr^{6+}$ molecules between the bulk solution and solid phase at equilibrium, namely Langmuir, Freundlich, Khan, and Dubinin-Randushkevich (Al-Ghouti and Da'ana, 2020). The mathematical form of the Langmuir equation is expressed in equation (6).

$$Q_e = Q_{\text{Lang}} \frac{K_{\text{Lang}} C_e}{(1 + K_{\text{Lang}} C_e)} \tag{6}$$

$Q_{\text{Lang}}$ is the predicted maximum adsorption capacity (mg/g), and $K_{\text{Lang}}$ is the Langmuir adsorption constant (L/mg).

The mathematical expression of the Freundlich model is shown by equation (7).

$$Q_e = K_{\text{Fr}} C_e^{1/n_{\text{Fr}}} \tag{7}$$

$K_{\text{Fr}}$ is the Freundlich constant related to the adsorption capacity $((\text{mg}/\text{g})(\text{L}/\text{g})^{1/n_{\text{Fr}}})$, and $n_{\text{Fr}}$ is an empirical constant related to the adsorption intensity.

The form of the Khan isotherm equation is shown by equation (8).

$$Q_e = Q_K \frac{K_K C_e}{(1 + K_K C_e)^{n_K}} \tag{8}$$

$Q_K$ (mg/g) is the maximum adsorption capacity (mg/g), $n_K$ is the model exponent, and $K_K$ is the model constant.

Equation (9) shows the mathematical form of the Dubinin-Randushkevich model.

$$Q_e = Q_{\text{DR}} e^{-B_{\text{DR}} \varepsilon^2} \tag{9}$$

$$\varepsilon = RT \ln \left( 1 + \frac{1}{C_e/C_s} \right) \tag{10}$$

$$E = \frac{1}{\sqrt{2 B_{\text{DR}}}} \tag{11}$$

$Q_{\text{DR}}$ is the maximum adsorption capacity (mg/g), $B_{\text{DR}}$ ($\text{mol}^2/\text{kJ}^2$) is the constant related to the adsorption energy, $\varepsilon$ (kJ/mol) is adsorption potential which is calculated as equation (10), $R$ is the ideal gas constant (8.314 J/mol K), $T$ is the absolute temperature (K), $C_s$ represents the solubility (mg/L), and $E$ (kJ/mol) is the mean free energy.

## 3. Results and discussion

### 3.1. Material characterization

The difference morphology and surface properties of DR, DR-Cel, and DR-AC were evaluated using characterization techniques including SEM, $N_2$ sorption isotherm, XRD, and FTIR. The surface morphology of the samples, as revealed by SEM imaging, is presented in Fig. 2. The DR appears to have several slab-like layers with a fairly smooth surface due to the wax content, and no porous structure is observed (Fig. 2a). In contrast to DR, DR-Cel has a more fibrous appearance (Fig. 2c) which can be attributed to the pulping process and subsequent removal of lignin and hemicellulose. Fig. 2b and d compare the morphology of DR and DR-Cel fiber. DR-Cel fibers look rougher than DR fibers due to the loss of lignin and wax during alkali treatment, which causes cracking (highlighted by yellow arrows in Fig. 2d). A similar phenomenon was reported by Obeng et al. (2021). The carbonization process of DR produces DR-AC with channels resembling pores that are visible from the fractured material (Fig. 2e). The other part of the DR-AC (Fig. 2f) only shows the appearance of particles with a rough surface without any unique morphological characteristics.

The functional group content in DR, DR-Cel, and DR-AC was described in FTIR spectra in Fig. 3a. DR and DR-Cel have similar FTIR spectra; however, some peaks are slightly shifted and have different intensities. For DR and DR-Cel, the broad peak at near 3350 cm$^{-1}$ can be assigned to the O-H stretching vibration of alcohol groups derived from lignin, cellulose, and hemicellulose. The peak at ~2900 cm$^{-1}$ for DR and DR-Cel corresponds to the symmetric C-H stretching vibration of the alkene groups. The peak at 1603 and 1634 cm$^{-1}$ for DR and DR-Cel, respectively, are associated with aromatic ring vibration of lignin and extractives. The peak at 1254 cm$^{-1}$ in DR spectra corresponds to O-H in-plane bending of the lignin; this peak disappears in the DR-Cel spectra, implying the reduced lignin content. The peak at ~890 cm$^{-1}$ in DR and DR-Cel is associated with the C-H rocking. The characteristic band of DR-Cel agrees with the reported literature (Javier-Astete et al., 2021). In DR-AC spectra, two spectra peaked at 3680 and 2630 cm$^{-1}$ is attributed to the stretching vibration of the O-H group of alcohol, phenols, and carboxylic acid. Another spectrum found at wavenumber 1658 cm$^{-1}$ represents the C=O stretching vibration. The peak at 1412 cm$^{-1}$ can be attributed to the bending vibration of O-H. The peak at 979 cm$^{-1}$ is assigned to the out-of-plane deformation mode of C-H of the benzene ring. The peak at 2900 cm$^{-1}$ observed in DR and DR-Cel disappeared in DR-AC, possibly due to the loss of hydrocarbon content during carbonization (Ukkakimapan et al., 2020).

The diffractogram of DR, DR-Cel, and DR-AC are given in Fig. 3b. DR
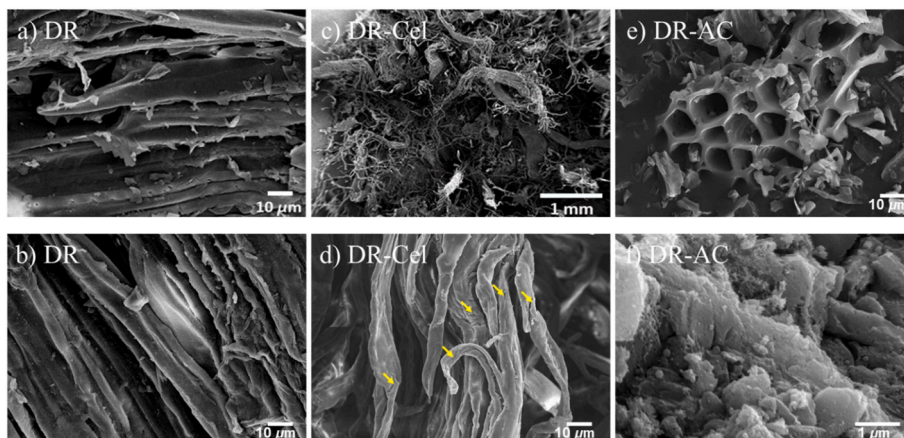


**Fig. 2.** The surface morphology of DR, DR-Cel, and DR-AC at different sections of the material.
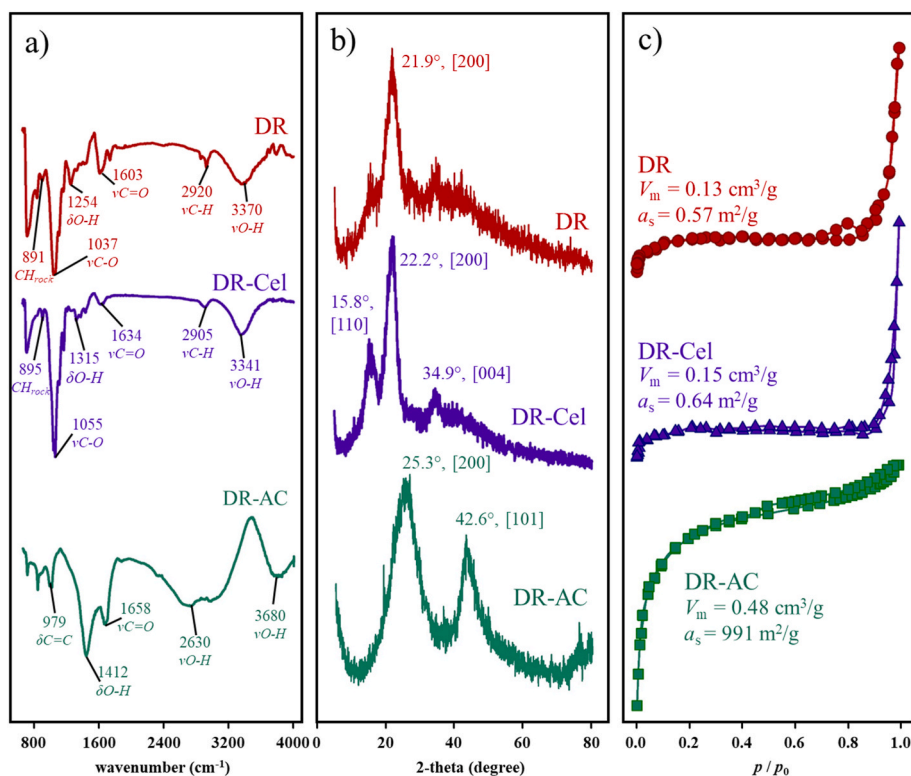
**Fig. 3.** Characterization of durian rind DR, DR-Cel, DR-AC. **a)** FTIR spectrum. **b)** XRD crystallinity pattern. **c)** $N_2$ sorption isotherm curve and the BET parameters.

mainly displayed an intense peak at 21.9°, corresponding to the [200] crystal plane of cellulose. The diffractogram of DR-Cel shows two peaks related to the crystallographic planes of cellulose in the direction of 15.8° and 22.2°, in accordance with the Bragg angles at 15.0° (plane [110]) and 22.8° (plane [200]) as indicated from International Centre for Diffraction Data (ICDD) with JCPDS number 50–2241. In addition, a peak at 34.9° associated with the crystal plane [004] was observed for DR-Cel, similar to that reported by Pusty and Shirage (2020). The observed crystallinity pattern of DR-AC was significantly different from that of DR and DR-Cel. Two sharp peaks were observed at 25.8° and 43.5°, corresponding to the crystal planes [200] and [101], respectively; this pattern is in good agreement with the AC from hemp straw reported by Shi et al. (2018).

The BET model was applied to evaluate the $N_2$ sorption isotherm for the DR, DR-C, and DR-AC (Fig. 3c). DR and DR-Cel show a type II isotherm, typical for non-porous materials. A significant change in the shape of the isotherm curve was observed after the DR was converted to DR-AC. DR-AC shows a type IV isotherm curve with hysteresis, indicating the presence of micropores and mesopores (Sotomayor et al., 2018). The existence of the micropore structure is further emphasized by the steep micropore filling section at low $p/p_0$. The BET modeling revealed the specific surface area ($a_s$) of DR, DR-Cel, and DR-AC, that is, 0.57, 0.64, and 991 $m^2/g$, respectively. The carbonization of DR into DR-AC created microporous and mesoporous structures of the material, which led to a significant increase in the $a_s$. The $a_s$ of biomass-based AC is varied as it is influenced by the type of original biomass and activating agent (Supplementary Information Table S1). The acid-activated AC exhibits a very high $a_s$, for example, the durian rind AC activated with HCl has $a_s$ of 1015 $m^2/g$, the fox nutshell AC activated with $H_3PO_4$ has $a_s$ of 2363 $m^2/g$. Meanwhile, the base-activated AC exhibits lower $a_s$ (226–1305 $m^2/g$). The AC from Brewer's spent grain with subsequent $H_3PO_4$ and KOH activation exhibits $a_s$ of 692.3 $m^2/g$. It is noted that the $a_s$ of activated carbon from DR produced in this work is comparable to that reported.

### 3.2. Adsorption study

#### 3.2.1. Effect of pH and initial adsorbate concentration

The change of pH influences the surface charge of the adsorbent and the speciation of the adsorbate, which in response, may affect the adsorbate-adsorbent interaction. The effect of pH on the removal efficiency (%removal) of $Cr^{6+}$ by DR, DR-Cel and DR-AC is shown in Fig. 4a. Optimum $Cr^{6+}$ removal was observed at an initial pH of 2 for all adsorbents, and it decreased with the increase in initial pH from 2 to 10. This phenomenon can be attributed to the tendency of pH-dependent properties of $Cr^{6+}$ and adsorbents (Anthony and Oladoja, 2021). At acidic pH, there is a high number of $H^+$ in the solution (Mudasir et al., 2020); thus, the surface charge of the adsorbent tends to be positive. On the other hand, the $Cr^{6+}$ ion is present in an anionic form in all pH ranges; specifically, $HCrO_4^-$ and $Cr_2O_7^{2-}$ at pH < 6 and $CrO_4^{2-}$ at pH > 6. Underlining these conditions, the adsorbent and $Cr^{6+}$ were present in opposite charge that promotes their interaction at acidic pH. The adsorbate and adsorbent at alkaline pH tend to be negatively charged, and therefore, higher repulsion interaction and less adsorption occur.

Fig. 4b shows the effect of the initial concentration of $Cr^{6+}$ on the % removal. A high %removal (~90%) can be reached at any initial concentration up to 100 mg/L. However, this efficiency gradually decreased as the initial concentration of $Cr^{6+}$ was increased (>100 mg/L). This phenomenon can be attributed to the limited number of adsorbent adsorption sites. At a high initial concentration, the amount of $Cr^{6+}$ exceeds the number of adsorption sites so that not all can be accommodated, resulting in a decrease in the % removal. Once equilibrium is reached, the absorption of excess adsorbate molecules is delayed because the adsorbent is saturated. At a low initial concentration, the amount of $Cr^{6+}$ present in the solution is proportional to the number of adsorption sites of the adsorbent. Therefore, almost all $Cr^{6+}$ ions can be accommodated.

#### 3.2.2. Kinetic study

The effect of contact time on the equilibrium adsorption capacity of
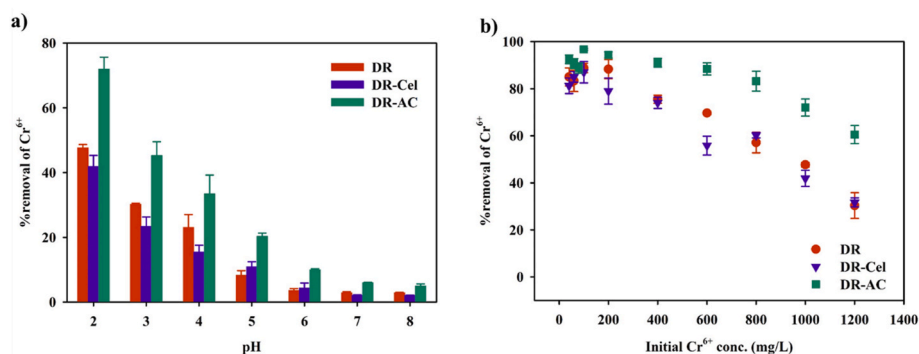
**Fig. 4.** Adsorption system of $Cr^{6+}$ using DR, DR-Cel, and DR-AC as adsorbents. **a)** Effect of pH (1000 mg/L, 30 °C, 8h) and **b)** effect of initial sorbate concentration (30 °C, pH 2, 8h).

$Cr^{6+}$ by each adsorbent was evaluated through a kinetic study (Fig. 5). A steep increase in $Q_t$ was observed within 100 min of contact, indicating rapid adsorption for all adsorbents due to the high affinity as all adsorption sites were vacant. It is worth noting that there is a steeper increase in the $Q_t$ of DR-AC compared to DR and DR-Cel, indicating the faster adsorption of $Cr^{6+}$ onto DR-AC. The $Q_t$ of $Cr^{6+}$ onto DR-AC reached its equilibrium (130 mg/g) and plateaued after 100 min. On the other hand, a gradual increase of Qt was still observed for DR and DR-Cel up to 400 min, and the adsorption equilibrium of DR (105 mg/g) and DR-Cel (110 mg/g) was only achieved after 480 min. The faster adsorption rate of DR-AC might be attributed to its greater $a_s$ (~1600-

fold) compared to DR and DR-Cel (refer to Supplementary Information Table S1), thus, allowing better contact with the $Cr^{6+}$ ions. The kinetic data fitting using P1O, P2O, Elovich, and IPD models was used to evaluate the adsorption rate and rate-limiting step of each adsorbent (Agbovi and Wilson, 2021); the kinetic data and its fittings are shown in Fig. 5. The calculated parameters based on the models are presented in Table 1. The adsorption of $Cr^{6+}$ by DR, DR-Cel, and DR-AC correlated well to P2O than P1O, which was indicated by higher $R^2$ and lower SSE values.

The solid fitting-line of P2O passing through all the kinetic data points, further confirms the high correlation of the model; on the other
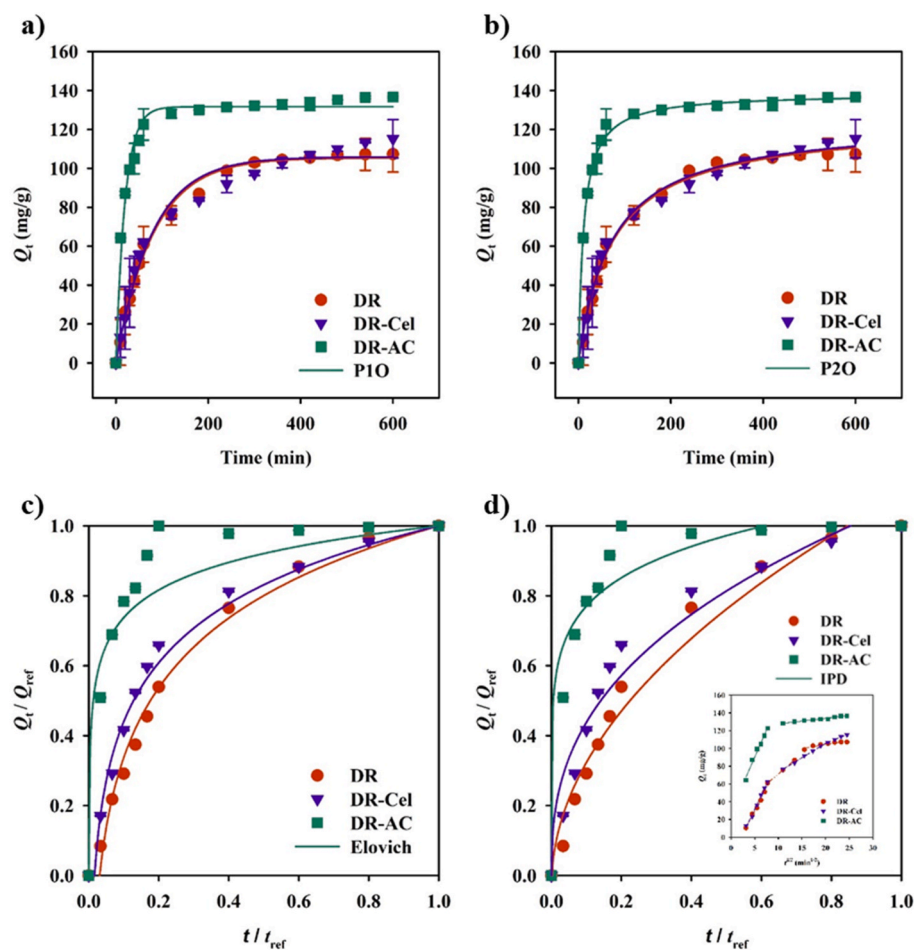


**Fig. 5.** Kinetic adsorption of $Cr^{6+}$ using DR, DR-Cel, and DR-AC. The solid lines show the data fitting using kinetic models of **a)** P1O, **b)** P2O, **c)** non-linear Elovich, and **d)** non-linear IPD and linear IPD (inset figure).

**Table 1**
Calculated parameters of P1O, P2O, Elovich, and IPD models for the adsorption of $Cr^{6+}$ on DR, DR-Cel, and DR-AC.

| Model | Parameter | Adsorbent | | | | | | | | |
|---|---|---|---|---|---|---|---|---|---|---|
| | | DR | | | DR-Cel | | | DR-AC | | |
| P1O | Q1 (mg/g) | 105.4 | ± | 1.333 | 105.9 | ± | 2.585 | 131.7 | ± | 1.687 |
| | k1 (min-1) | 0.012 | ± | 0.001 | 0.013 | ± | 0.001 | 0.050 | ± | 0.003 |
| | R2 | 0.993 | | | 0.972 | | | 0.979 | | |
| | SSE | 147.5 | | | 565.5 | | | 385.5 | | |
| P2O | Q2 (mg/g) | 123.9 | ± | 1.901 | 124.7 | ± | 2.407 | 138.6 | ± | 0.862 |
| | k2 (g/mg min) × 104 | 1.103 | ± | 0.008 | 1.119 | ± | 0.010 | 6.322 | ± | 0.029 |
| | R2 | 0.995 | | | 0.992 | | | 0.997 | | |
| | SSE | 103.8 | | | 170.3 | | | 62.01 | | |
| Elovich | RE | 0.288 | ± | 0.006 | 0.243 | ± | 0.005 | 0.114 | ± | 0.012 |
| | R2 | 0.991 | | | 0.992 | | | 0.944 | | |
| | SSE | 0.012 | | | 0.008 | | | 0.052 | | |
| IPD | RIPD | 0.990 | ± | 0.103 | 0.871 | ± | 0.091 | 0.531 | ± | 0.057 |
| | R2 | 0.972 | | | 0.938 | | | 0.944 | | |
| | SSE | 0.057 | | | 0.099 | | | 0.398 | | |
| | *First segment* | | | | | | | | | |
| | Ci,1 | −20.34 | ± | 2.784 | −24.21 | ± | 2.900 | 29.44 | ± | 4.838 |
| | ki,1 | 9.965 | ± | 0.508 | 11.18 | ± | 0.490 | 12.15 | ± | 0.818 |
| | R2 | 0.990 | | | 0.990 | | | 0.978 | | |
| | SSE | 7.340 | | | 13.89 | | | 38.66 | | |
| | *Second segment* | | | | | | | | | |
| | Ci,2 | 25.56 | ± | 0.293 | 40.99 | ± | 1.504 | 121.4 | ± | 0.824 |
| | ki,2 | 4.577 | ± | 0.027 | 3.239 | ± | 0.092 | 0.621 | ± | 0.043 |
| | R2 | 1.000 | | | 0.996 | | | 0.962 | | |
| | SSE | 0.012 | | | 2.116 | | | 2.208 | | |
| | *Third segment* | | | | | | | | | |
| | Ci,3 | 86.59 | ± | 2.916 | 65.45 | ± | 7.432 | – | | |
| | ki,3 | 0.893 | ± | 0.142 | 1.041 | ± | 0.320 | – | | |
| | R2 | 0.865 | | | 0.952 | | | – | | |
| | SSE | 6.339 | | | 0.342 | | | – | | |

hand, the P1O model fitting under or overestimates the experimental data points close to equilibrium. The rate constant of $Cr^{6+}$ adsorption by DR, DR-Cel, and DR-AC was assessed based on the time-scaling factor of the P2O model ($k_2$), and the adsorption rate followed the order DR-AC > DR-Cel > DR. The faster adsorption by DR-AC was attributed to micro- and mesoporous structures that enable more efficient contact with $Cr^{6+}$. The kinetics adsorption data were further evaluated using the Elovich dimensionless parameters, $R_E$. All adsorbents showed a $R_E$ value of 0.3 > $R_E$ > 0.1 which corresponds to zone II of mildly rising adsorption (Wu et al., 2009a,b). The lower $R_E$ indicates that the system is faster in reaching equilibrium. The $R_E$ of DR-AC is the lowest compared to DR-Cel and DR, implying the faster uptake of $Cr^{6+}$, in good agreement with the P2O model.

The dimensionless initial adsorption factor of the IPD model ($R_{IPD}$) describes the initial adsorption behavior of an adsorbent (Wu et al., 2009a,b), where the $R_{IPD}$ of DR is 0.990, indicating slow initial adsorption. The $R_{IPD}$ of DR-Cel is 0.871, displaying an intermediate initial adsorption behavior. The $R_{IPD}$ of DR-AC is 0.531, indicating rapid initial adsorption. The linear-IPD model fitting was employed on the kinetic adsorption data to evaluate the mass transfer steps (Wang and Guo, 2020). The first segment with a steep slope can be attributed to the external surface adsorption between the hydrated adsorbent and the outermost adsorption sites. The diffusion rate constant of the first segment ($k_{i,1}$) follows the order of DR-AC > DR-Cel > DR. The negative intercept ($C_{i,1}$) for DR and DR-Cel indicates the presence of internal film diffusion, which creates a boundary layer effect (Wu et al., 2009a,b), leading to slower solute uptake. The second segment is the gradual adsorption step which occurs as the solute moves towards smaller pores; thus, the uptake was slowed down (Schwaab et al., 2017). In this second segment, $k_{i,2}$ for DR and DR-Cel are higher than DR-AC, indicating the faster solute uptake by DR and DR-Cel. This can be attributed to the swelling phenomenon of the DR and DR-Cel polymer chains due to extended hydration time. Swelling of polymer chains causes surface pores to expand (Ha et al., 2018), thus, creating a greater surface area of the adsorbent and increasing the $Cr^{6+}$ uptake. The third linear segment

was observed for DR and DR-Cel ascribed to the internal film diffusion.

*3.2.3. Isotherm study*

The isotherm study reveals the equilibrium behavior of solute or adsorbate, which is crucial for designing an efficient adsorption system. The isotherm data for $Cr^{6+}$ uptake by DR, DR-Cel, and DR-AC at 30 °C and their isotherm model fitting are presented in Fig. 6. The parameters from Langmuir, Freundlich, Khan, and Dubinin-Radushkevich fitting are given in Table 2, with the Khan isotherm model providing the highest fit to the three adsorption systems, as indicated by the high $R^2$ and lower SSE. The maximum adsorption capacity for $Cr^{6+}$ follows the order of DR-AC > DR-Cel > DR, with $Q_K$ 223.3, 154.2, and 124.5 mg/g, respectively. The high adsorption capacity of DR-AC is attributed to its micro- and mesoporous structure. The higher $K_K$ parameter for DR-AC than DR and DR-Cel indicates that this adsorbent has a higher adsorption affinity for $Cr^{6+}$. This also explains the faster $Cr^{6+}$ adsorption rate by DR-AC compared to DR and DR-Cel (as described previously in kinetic studies). The exponential parameter $n_K$ exhibits a value of ~1 for all systems, approach to unity, indicating homogenous adsorption behavior of $Cr^{6+}$ by DR, DR-Cel, and DR-AC. Dubinin-Randushkevich model was employed to estimate the mean free energy ($E$) of the adsorption systems. The calculation on the $E$ parameter of all adsorbents shows the value < 8 kJ/mol, suggesting the physical adsorption feature of the systems (Zhou et al., 2021).

The $Q_{max}$ of DR, DR-Cel, and DR-AC toward $Cr^{6+}$ is comparable to that of other biomass-derived adsorbents (Supplementary Information Table S2). The $Q_{max}$ of DR (124.5 mg/g) falls short compared to the Carob waste (212.4 mg/g), which might be attributed to the different porosity of the two biomasses. Bouaouina et al. (2022) showed that the Carob waste is a mesoporous material; meanwhile, the DR tends to be non-porous and therefore has a smaller $Q_{max}$. Nevertheless, DR waste is deemed more economically valued due to its local availability in Indonesia; here, DR waste is under-appreciated and in greater abundance than Carob waste. Unlike the DR, the DR-Cel possesses greater $Q_{max}$ (154.2 mg/g) than other celluloses, for example, the waste cotton
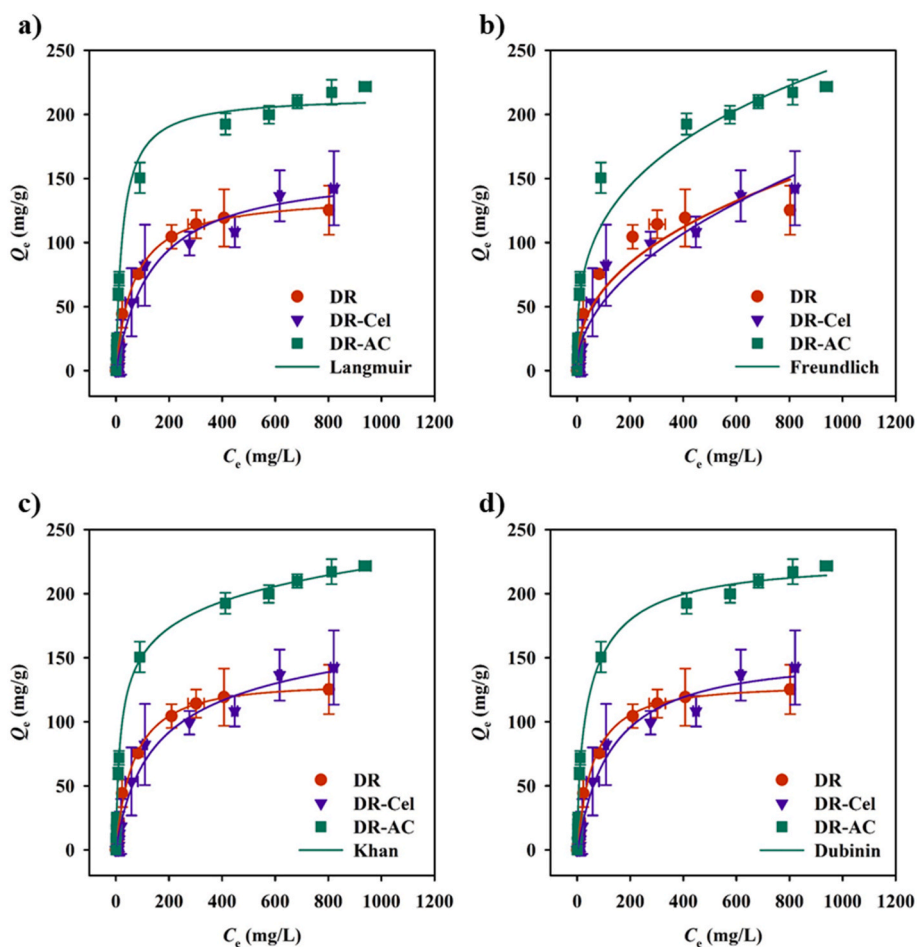
**Fig. 6.** Isotherm adsorption system of $Cr^{6+}$ using DR, DR-Cel, and DR-AC as adsorbents. The solid lines show the data fitting using various kinetic models: **a)** Langmuir, **b)** Freundlich, **c)** Khan, and **d)** Dubinin-Randushkevich.

**Table 2**
Calculated parameter of Langmuir, Freundlich, Khan, and Dubinin-Randushkevich isotherm model for adsorption of $Cr^{6+}$ on DR, DR-Cel, and DR-AC.

| Model | Parameter | Adsorbent | | | | | | | | |
|---|---|---|---|---|---|---|---|---|---|---|
| | | DR | | | DR-Cel | | | DR-AC | | |
| Langmuir | $Q_{Lang}$ (mg/g) | 138.0 | ± | 4.156 | 159.3 | ± | 9.254 | 214.7 | ± | 4.064 |
| | $k_{Lang}$ (L/mg) | 0.015 | ± | 0.002 | 0.017 | ± | 0.001 | 0.039 | ± | 0.005 |
| | $R^2$ | 0.991 | | | 0.978 | | | 0.992 | | |
| | SSE | 559.7 | | | 771.3 | | | 779.5 | | |
| Freundlich | $K_{Fr}$ (L/g) | 9.474 | ± | 2.890 | 5.455 | ± | 1.785 | 27.77 | ± | 4.863 |
| | $n_{Fr}$ | 2.426 | ± | 0.305 | 2.013 | ± | 0.215 | 3.212 | ± | 0.286 |
| | $R^2$ | 0.915 | | | 0.945 | | | 0.968 | | |
| | SSE | 2557 | | | 1922 | | | 3185 | | |
| Khan | $Q_K$ (mg/g) | 124.5 | ± | 62.55 | 154.2 | ± | 30.60 | 223.3 | ± | 6.030 |
| | $K_K$ | 0.011 | ± | 0.008 | 0.013 | ± | 0.004 | 0.095 | ± | 0.008 |
| | $n_K$ | 0.868 | ± | 0.182 | 1.047 | ± | 0.086 | 0.869 | ± | 0.009 |
| | $R^2$ | 0.977 | | | 0.991 | | | 0.999 | | |
| | SSE | 701.9 | | | 251.8 | | | 48.81 | | |
| Dubinin-Radushkevich | $Q_{DR}$ (mg/g) | 128.0 | ± | 6.003 | 148.2 | ± | 13.58 | 223.0 | ± | 5.587 |
| | $B_{DR}$ (mol$^2$/J$^2$) × 10$^5$ | 8.980 | ± | 0.005 | 8.370 | ± | 0.009 | 5.020 | ± | 0.008 |
| | $Cs$ (mg/L) | 453.1 | ± | 229.0 | 1088 | ± | 760.3 | 1243 | ± | 452.9 |
| | $E$ (kJ/mol) | 0.075 | | | 0.077 | | | 0.099 | | |
| | $R^2$ | 0.992 | | | 0.975 | | | 0.997 | | |
| | SSE | 190.6 | | | 713.5 | | | 286.1 | | |

cellulose (82 mg/g), bacterial cellulose (5.13 mg/g), and styrene-modified cellulose microsphere (123.4 mg/g). However, the $Q_{max}$ of DR-Cel is lower than the one modified using magnetic nanoparticles (171.5 mg/g). Despite the slightly lower $Q_{max}$ (~10% lower), the preparation of DR-Cel is less complex, with no additional modification steps; thus, it is economically sound. Similarly, DR-AC has superior $Q_{max}$ (223.2 mg/g) comparable to or even higher than some of the other presented AC adsorbents, e.g., granular AC (45.2 mg/g), dried red algae AC (66 mg/g), *Enteromorpha prolifera* AC (88.17 mg/g), and glucose/dodecylbenzene sulfonate AC (230.15 mg/g).

### 3.3. Cost analysis

An economic assessment of a production system can provide an overview of the potential economic profitability of the system. The economic evaluation is carried out by adopting the LCCA (Wang et al., 2021) with several modifications. Specifically, the evaluation is applied to several interdependent phases, i.e., raw material cost (RMC), transportation cost (TC), and processing cost (PC), which are represented in the following Eq. (12).

$$LCC = RMC + TC + PC \tag{12}$$

The RMC includes purchasing raw materials from local waste disposal sites, chemicals (calculated separately in Table 3), and labor costs for manual collection. The TC consists of the cost of transporting raw materials and chemicals to the factory site. The PC was calculated as the total power requirement for the pretreatment and processing step, including the scenario of mixing, carbonization, activation, and drying. All calculation was performed using 1 ton of raw material as the basis. The steps in producing DR-Cel and DR-AC from DR are based directly on laboratory-scale methods (as mentioned in Sections 2.2 and 2.3).

The cost of raw materials and chemicals was evaluated as the direct operating costs (DOC), as presented in Table 3. The results of the DOC analysis show that it takes a cost of US\$ 2.3 to provide chemicals to process 1 kg of DR into DR-Cel. Meanwhile, US\$3.6 was required for providing the chemicals needed in DR-AC production, which is US\$ 1.3 higher than DR-Cel. The subsequent cost estimation by LCCA shows that the raw material cost has the most significant proportion in the cost component, ~80% of the total cost. The second-largest cost component is transportation; nevertheless, this cost can be minimized by purchasing chemicals from local suppliers. In DR-AC production, the cost of electricity required to run the primary process step (carbonization) is higher than that of DR-Cel. The cost of electricity needed to produce DR-AC is US\$ 30.34 from 1 ton of DR, which is ~6 times higher than DR-Cel. Based on the LCCA in Table 4, the cost of processing 1 ton of DR into DR-Cel is approximately US\$ 2848.23, equivalent to US\$ 2.9/kg. Meanwhile, to process 1 ton of DR into DR-AC, a cost of US\$ 4219.63 (US\$ 4.2/kg) is required, which is 1.5 times higher than DR-Cel.

The price of AC from the Chinese market varies between US\$1.8 to 5.2 per kg, while cellulose fiber is from US\$1.7 to 4.0 per kg; thus, the estimated product cost of this work still falls within the market price range. It is also worth mentioning that when cost minimization is needed, raw materials requiring less chemical processing can be selected. For example, a simple alkaline treatment using 8% NaOH is needed to purify cellulose from kapok (Zhang et al., 2022); a smaller amount of chemicals is required to obtain cellulose from coconut husk (Thinkohkaew et al., 2020). Meanwhile, to minimize the cost of materials in producing AC, the substitution of the KOH activation method by using cheaper compounds or acids can be done. In addition, the use of low-value waste also can reduce the cost of raw materials. for instance, several studies have reported the use of Brewer's spent grain (Osman et al., 2020a), herbaceous biomass (Osman et al., 2020b), spent coffee grounds (Mukherjee et al., 2022), organic fertilizers (Osman et al., 2022), etc. It is important to note the limitations of the above economic assessment, i.e., raw material and energy costs are closely related to inflation variables and resource costs in each country, so the calculation of production costs per ton of the raw materials used may vary depending on the market in each region. The economic evaluation in this study was carried out within the scenario with system boundaries, as given in Table 4. Alternative strategies (to minimize production costs), process optimization, reusability scenario, and life cycle carbon scenario were not included in this study.

The intermittent approach demonstrated by Penjumras et al. (2014) was applied to produce DR-Cell. This approach involves a stepwise attack on the hydrogen bonds of the lignocellulosic chains. For example, in the removal of lignin with NaOH solution: the first addition of NaOH solution gives hydroxyl ions to attack the hydrogen bonds and cause the bonds to weaken. As fresh NaOH solution is added, the next addition, new hydroxyl ions appear to attack the hydrogen bonds again. The effectiveness of intermittent addition vs. one-time addition of reagent in producing higher purity cellulose can be carried out in another detailed study. Meanwhile, carbonization was employed to prepare the DR-AC. This technique can be considered a cleaner production strategy for producing activated carbon; the oxygen-free combustion of this technique can mitigate NOx and SOx emissions (Osman, 2020).

### 4. Conclusion

Upcycling of DR biomass waste into DR-Cel and DR-AC were reported here. The resultant DR-derived materials showed adsorption potential with their uptake rate and capacity of $Cr^{6+}$ follow the order of DR-AC > DR-Cel > DR. The economic analysis indicates that raw materials and chemicals contribute the highest portion of the cost component. The carbonization process in the production of DR-AC requires high electrical consumption, impacting its power cost, whereas the mixing process for DR-Cel production requires low power. In this work, DR-Cel and DR-AC were prepared by directly adopting the previously reported methods without considering optimization or alternative techniques, which can be associated with high production costs. Nevertheless, both DR-Cel and DR-AC showed comparable adsorption capacities than previously reported adsorbents. Future in-depth studies should be carried out on the techno-economic assessment of various alternative strategies that can produce products with equivalent (or better) properties but at lower costs.

### CRediT authorship contribution statement

**Carlos David Sulistiyo:** Investigation, Data curation, Formal analysis, Writing – original draft. **Kuan-Chen Cheng:** Investigation, Data curation, Formal analysis, Writing – original draft. **Henoch Jaya Su'andi:** Investigation, Data curation, Formal analysis, Writing – original draft. **Maria Yuliana:** Formal analysis, Data curation. **Chang-Wei Hsieh:** Formal analysis, Data curation. **Suryadi Ismadji:** Resources, Writing – review & editing. **Artik Elisa Angkawijaya:** Conceptualization. **Alchris Woo Go:** Conceptualization. **Hsien Yi Hsu:** Conceptualization, Data curation, Writing – review & editing. **Phuong Lan Tran-Nguyen:** Supervision, Project administration. **Shella Permatasari Santoso:** Investigation, Funding acquisition, Writing – original draft, Writing – review & editing.

**Table 3**
The direct operating cost for scaled-up production of cellulose and activated carbon from durian rind.

| Material | Specification[a] | Price (US \$/kg) [b] | Amount[c] | | Total price (US\$) | |
|---|---|---|---|---|---|---|
| | | | | | Cellulose | Activated carbon |
| Durian rind (DR) | | 0.344[d] | 1 | kg | 0.344 | 0.344 |
| NaClO$_2$ | 25% | 0.550 | 1 | L | 0.550 | – |
| CH$_3$COOH | 99.9% | 0.590 | 2 | L | 1.180 | – |
| NaOH | 99% | 0.310 | 0.66 | kg | 0.204 | – |
| KOH | 90% | 0.820 | 4 | kg | – | 3.280 |
| **Total DOC** | | | | | 2.278 ≈ 2.3 | 3.624 ≈ 3.6 |

[a] Industrial grade material specifications.
[b] Price was based on Made-in-China, Focus Technology Co., Ltd. (https://www.made-in-china.com).
[c] The scale-up was based on the experimental procedure in sections 2.2 and 2.3.
[d] Price of durian rind was according to Indonesia market, with conversion rate 1 US\$ = IDR 14,661.

**Table 4**
Life-cycle cost analysis approach for scaled-up production of cellulose and activated carbon from durian rind.

| Scenario | Cellulose production | | | | Activated carbon production | | | |
|---|---|---|---|---|---|---|---|---|
| | Unit price (US$) | Qty. | Total cost (US$) | Description | Unit price (US$) | Qty. | Total cost (US$) | Description |
| Raw material and chemicals | 2278 | – | 2278 | Raw material and chemicals as listed in Table 1, with scale up to 1 ton of DR | 3624 | – | 3624 | Raw material and chemicals as listed in Table 1, with scale up to 1 ton of DR |
| Transportation (1) | 75 | 1 ton, 250 km | 75 | Logistic price for transporting ≤5 tons and distance 250 km | 75 | 1 ton, 250 km | 75 | Logistic price for transporting ≤5 tons and distance 250 km |
| Manual collection | 10 | 2 labors | 20 | Salary for 2 workers for manual collection of DR | 10 | 2 labors | 20 | Salary for 2 workers for manual collection of DR |
| Transportation (2) | 450 | – | 450 | Import tariffs taking into account ocean freight rates from China to Indonesia, with an expedition time of 8 days | 450 | – | 450 | Import tariffs taking into account ocean freight rates from China to Indonesia, with an expedition time of 8 days |
| *Electricity cost in Pretreatment* | | | | | | | | |
| Crushing | 0.079/kWh[a] | $P = 22$ kWh $t = 10$ min $C = 10$ t/h | 0.29 | 1 unit of hammer crusher was used to cut the DR into smaller pieces | 0.079/kWh[a] | $P = 22$ kWh $t = 10$ min $C = 10$ t/h | 0.29 | 1 unit of hammer crusher was used to cut the DR into smaller pieces |
| *Electricity cost in Processing* | | | | | | | | |
| Mixing (1) | 0.079/kWh[a] | $P = 1.1$ kWh $t = 300$ min $C = 2000$ L | 0.44 | Mixing of DR with $NaClO_2$ and $CH_3COOH$. | | | | |
| Mixing (2) | 0.079/kWh[a] | $P = 1.1$ kWh $t = 120$ min $C = 2000$ L | 0.17 | Mixing treated DR with NaOH. | | | | |
| Drying | – | – | – | – | 0.079/kWh[a] $t = 240$ min $C = 1000$ L | $P = 12$ kWh | 3.73 | Drying process to minimize water content |
| Carbonization | – | – | – | – | 0.079/kWh[a] | $P = 100$ kWh $t = 120$ min $C = 850$ L | 15.80 | Carbonization at 500 °C. |
| Activation | – | – | – | – | 0.079/kWh[a] | $P = 1.1$ kWh $t = 60$ min $C = 2000$ L | 0.09 | Impregnation with KOH |
| Drying | 0.079/kWh[a] $t = 240$ min $C = 1000$ L | $P = 12$ kWh | 3.73 | Drying process to obtain dried cellulose | 0.079/kWh[a] | $P = 100$ kWh $t = 60$ min $C = 850$ L | 7.90 | Char activation at 500 °C |
| Utility[b] | 1.080/m³[b] | 0.115 m³ | 0.13 | The cost of water for pretreatment and processing. The total volume of water is 115 L | 1.080/m³[b] | 0.034 m³ | 0.04 | The cost of water for pretreatment and processing. The total volume of water is 34 L |
| Energy loss | 0.079/kWh | – | 0.47 | The energy loss was estimated as 10% of the total power | 0.079/kWh | – | 2.78 | The energy loss was estimated as 10% of the total power |
| Other | – | – | 20.00 | Considering additional costs manual filling material, pickup, etc. | | | 20.00 | Considering additional costs manual filling material, pickup, etc. |
| | | 2848.23 | The estimated total cost for processing 1 ton of DR into cellulose | | | | 4219.63 | The estimated total cost for processing 1 ton of DR into activated carbon |

[a] Tariff for industrial electrical per kWh, for usage more than 200 kVA
[b] Tariff for industrial water per m³ for usage 0–10 m³.

## Declaration of competing interest

## Data availability

Data will be made available on request.

## Acknowledgments

## Appendix A. Supplementary data

Supplementary data to this article can be found online at https://doi.org/10.1016/j.jclepro.2022.135010.

## References

Abreu, P.L., Cunha-Oliveira, T., Ferreira, L.M.R., Urbano, A.M., 2018. Hexavalent chromium, a lung carcinogen, confers resistance to thermal stress and interferes with heat shock protein expression in human bronchial epithelial cells. Biometals 31, 477–487. https://doi.org/10.1007/s10534-018-0093-7.

Agbovi, H.K., Wilson, L.D., 2021. In: Kalia, S. (Ed.), 1 - Adsorption Processes in Biopolymer Systems: Fundamentals to Practical Applications. Elsevier, pp. 1–51.

Ahmed, M.B., Hasan Johir, M.A., Zhou, J.L., Ngo, H.H., Nghiem, L.D., Richardson, C., Moni, M.A., Bryant, M.R., 2019. Activated carbon preparation from biomass feedstock: clean production and carbon dioxide adsorption. J. Clean. Prod. 225, 405–413. https://doi.org/10.1016/j.jclepro.2019.03.342.

Al-Ghouti, M.A., Da'ana, D.A., 2020. Guidelines for the use and interpretation of adsorption isotherm models: a review. J. Hazard Mater. 393, 122383 https://doi.org/10.1016/j.jhazmat.2020.122383.

Anthony, E.T., Oladoja, N.A., 2021. Process enhancing strategies for the reduction of Cr (VI) to Cr(III) via photocatalytic pathway. Environ. Sci. Pollut. Res. 29, 8026–8053.

Bisara, D., Muchtar, J., 2018. Indonesia on the Cusp of its First Durian Surplus in Nine Years. Jakarta Globe, Jakarta, Jakarta Globe.

Bouaouina, K., Barras, A., Bezzi, N., Amin, M.A., Szunerits, S., Boukherroub, R., 2022. Adsorption-reduction of Cr(VI) onto unmodified and phytic acid-modified carob waste: kinetic and isotherm modeling. Chemosphere 297, 134188. https://doi.org/10.1016/j.chemosphere.2022.134188.

Chintagunta, A.D., Zuccaro, G., Kumar, M., Kumar, S.P.J., Garlapati, V.K., Postemsky, P. D., Kumar, N.S.S., Chandel, A.K., Simal-Gandara, J., 2021. Biodiesel production from lignocellulosic biomass using oleaginous microbes: prospects for integrated biofuel production. Front. Microbiol. 12 https://doi.org/10.3389/fmicb.2021.658284.

Davies, G., El Sheikh, A., Collett, C., Yakub, I., McGregor, J., 2021. In: Sadjadi, S. (Ed.), Chapter 5 - Catalytic Carbon Materials from Biomass. Elsevier, pp. 161–195.

Gill, M.K., Kocher, G.S., Panesar, A.S., 2021. Optimization of acid-mediated delignification of corn stover, an agriculture residue carbohydrate polymer for improved ethanol production. Carbohydrate Polymer Technologies and Applications 2, 100029. https://doi.org/10.1016/j.carpta.2020.100029.

Ha, J., Kim, J., Jung, Y., Yun, G., Kim, D.-N., Kim, H.-Y., 2018. Poro-elasto-capillary wicking of cellulose sponges. Sci. Adv. 4, eaao7051.

Islam, M.A., Angove, M.J., Morton, D.W., 2019. Recent innovative research on chromium (VI) adsorption mechanism. Environ. Nanotechnol. Monit. Manag. 12, 100267 https://doi.org/10.1016/j.enmm.2019.100267.

Javier-Astete, R., Jimenez-Davalos, J., Zolla, G., 2021. Determination of hemicellulose, cellulose, holocellulose and lignin content using FTIR in *Calycophyllum spruceanum* (Benth.) K. Schum. and *Guazuma crinita* Lam. PLoS One 16, e0256559. https://doi.org/10.1371/journal.pone.0256559.

Lace, A., Ryan, D., Bowkett, M., Cleary, J., 2019. Chromium monitoring in water by colorimetry using optimised 1,5-diphenylcarbazide method. Int. J. Environ. Res. Publ. Health 16, 1803. https://doi.org/10.3390/ijerph16101803.

Mudasir, M., Baskara, R.A., Suratman, A., Yunita, K.S., Perdana, R., Puspitasari, W., 2020. Simultaneous adsorption of Zn(II) and Hg(II) ions on selective adsorbent of dithizone-immobilized bentonite in the presence of Mg(II) ion. J. Environ. Chem. Eng. 8, 104002 https://doi.org/10.1016/j.jece.2020.104002.

Mukherjee, A., Okolie, J.A., Niu, C., Dalai, A.K., 2022. Techno – economic analysis of activated carbon production from spent coffee grounds: comparative evaluation of different production routes. Energy Convers. Manag. 14, 100218 https://doi.org/10.1016/j.ecmx.2022.100218.

Ngabura, M., Hussain, S.A., Ghani, W.A.W.A., Jami, M.S., Tan, Y.P., 2018. Utilization of renewable durian peels for biosorption of zinc from wastewater. J. Environ. Chem. Eng. 6, 2528–2539. https://doi.org/10.1016/j.jece.2018.03.052.

Obeng, A.K., Premjet, D., Premjet, S., 2018. Fermentable sugar production from the peels of two durian (durio zibethinus Murr.) cultivars by phosphoric acid pretreatment. Resources 7. https://doi.org/10.3390/resources7040060.

Obeng, A.K., Premjet, D., Premjet, S., 2021. Improved glucose recovery from durian peel by alkaline-catalyzed steam pretreatment. PeerJ 9, e12026. https://doi.org/10.7717/peerj.12026.

Offei, F., Koranteng, L.D., Kemausuor, F., 2021. Integrated bioethanol and briquette recovery from rice husk: a biorefinery analysis. Biomass Convers. Biorefin. https://doi.org/10.1007/s13399-021-01731-3.

Osman, A.I., 2020. Mass spectrometry study of lignocellulosic biomass combustion and pyrolysis with NOx removal. Renew. Energy 146, 484–496. https://doi.org/10.1016/j.renene.2019.06.155.

Osman, A.I., O'Connor, E., McSpadden, G., Abu-Dahrieh, J.K., Farrell, C., Al-Muhtaseb, A.a.H., Harrison, J., Rooney, D.W., 2020a. Upcycling brewer's spent grain waste into activated carbon and carbon nanotubes for energy and other applications via two-stage activation. J. Chem. Technol. Biotechnol. 95, 183–195. https://doi.org/10.1002/jctb.6220.

Osman, A.I., Farrell, C., Al-Muhtaseb, A.a.H., Harrison, J., Rooney, D.W., 2020b. The production and application of carbon nanomaterials from high alkali silicate herbaceous biomass. Sci. Rep. 10, 2563. https://doi.org/10.1038/s41598-020-59481-7.

Osman, A.I., Fawzy, S., Farghali, M., El-Azazy, M., Elgarahy, A.M., Fahim, R.A., Maksoud, M.I.A.A., Ajlan, A.A., Yousry, M., Saleem, Y., Rooney, D.W., 2022. Biochar for agronomy, animal farming, anaerobic digestion, composting, water treatment, soil remediation, construction, energy storage, and carbon sequestration: a review. Environ. Chem. Lett. 20, 2385–2485. https://doi.org/10.1007/s10311-022-01424-x.

Peng, H., Guo, J., 2020. Removal of chromium from wastewater by membrane filtration, chemical precipitation, ion exchange, adsorption electrocoagulation, electrochemical reduction, electrodialysis, electrodeionization, photocatalysis and nanotechnology: a review. Environ. Chem. Lett. 18, 2055–2068. https://doi.org/10.1007/s10311-020-01058-x.

Pusty, M., Shirage, P.M., 2020. Gold nanoparticle–cellulose/PDMS nanocomposite: a flexible dielectric material for harvesting mechanical energy. RSC Adv. 10, 10097–10112. https://doi.org/10.1039/C9RA10811D.

Revellame, E.D., Fortela, D.L., Sharp, W., Hernandez, R., Zappi, M.E., 2020. Adsorption kinetic modeling using pseudo-first order and pseudo-second order rate laws: a review. Cleaner Eng. Technol. 1, 100032 https://doi.org/10.1016/j.clet.2020.100032.

Schwaab, M., Steffani, E., Barbosa-Coutinho, E., Severo Júnior, J.B., 2017. Critical analysis of adsorption/diffusion modelling as a function of time square root. Chem. Eng. Sci. 173, 179–186. https://doi.org/10.1016/j.ces.2017.07.037.

Shi, G., Liu, C., Wang, G., Chen, X., Li, L., Jiang, X., Zhang, P., Dong, Y., Jia, S., Tian, H., Liu, Y., Wang, Z., Zhang, Q., Zhang, H., 2018. Preparation and electrochemical performance of electrospun biomass-based activated carbon nanofibers. Ionics 25, 1805–1812. https://doi.org/10.1007/s11581-018-2675-3.

Sotomayor, F.J., Cychosz, K.A., Thommes, M., 2018. Characterization of micro/mesoporous materials by physisorption: concepts and case studies. Accounts Mater. Surface Res. 3, 34–50.

Tan, Y.L., Abdullah, A.Z., Hameed, B.H., 2017. Fast pyrolysis of durian (Durio zibethinus L) shell in a drop-type fixed bed reactor: pyrolysis behavior and product analyses. Bioresour. Technol. 243, 85–92. https://doi.org/10.1016/j.biortech.2017.06.015.

Thinkohkaew, K., Rodthongkum, N., Ummartyotin, S., 2020. Coconut husk (Cocos nucifera) cellulose reinforced poly vinyl alcohol-based hydrogel composite with control-release behavior of methylene blue. J. Mater. Res. Technol. 9, 6602–6611. https://doi.org/10.1016/j.jmrt.2020.04.051.

Ukkakimapan, P., Sattayarut, V., Wanchaem, T., Yordsri, V., Phonyiem, M., Ichikawa, S., Obata, M., Fujishige, M., Takeuchi, K., Wongwiriyapan, W., Endo, M., 2020. Preparation of activated carbon via acidic dehydration of durian husk for supercapacitor applications. Diam. Relat. Mater. 107, 107906 https://doi.org/10.1016/j.diamond.2020.107906.

Wang, J., Guo, X., 2020. Adsorption kinetic models: physical meanings, applications, and solving methods. J. Hazard Mater. 390, 122156 https://doi.org/10.1016/j.jhazmat.2020.122156.

Wang, T., Li, G., Yang, K., Zhang, X., Wang, K., Cai, J., Zheng, J., 2021. Enhanced ammonium removal on biochar from a new forestry waste by ultrasonic activation: characteristics, mechanisms and evaluation. Sci. Total Environ. 778, 146295 https://doi.org/10.1016/j.scitotenv.2021.146295.

Wu, F.-C., Tseng, R.-L., Juang, R.-S., 2009a. Characteristics of Elovich equation used for the analysis of adsorption kinetics in dye-chitosan systems. Chem. Eng. J. 150, 366–373. https://doi.org/10.1016/j.cej.2009.01.014.

Wu, F.-C., Tseng, R.-L., Juang, R.-S., 2009b. Initial behavior of intraparticle diffusion model used in the description of adsorption kinetics. Chem. Eng. J. 153, 1–8. https://doi.org/10.1016/j.cej.2009.04.042.

Zhang, H., Zhao, T., Chen, Y., Hu, X., Xu, Y., Xu, G., Wang, F., Wang, J., Shen, H., 2022. A sustainable nanocellulose-based superabsorbent from kapok fiber with advanced oil absorption and recyclability. Carbohydr. Polym. 278, 118948 https://doi.org/10.1016/j.carbpol.2021.118948.

Zhou, Y., Li, Y., Liu, D., Liu, D., Xu, L., Liu, C., 2021. Adsorption optimization of uranium (VI) onto polydopamine and sodium titanate co-functionalized MWCNTs using response surface methodology and a modeling approach. Colloids Surf. A Physicochem. Eng. Asp. 627, 127145 https://doi.org/10.1016/j.colsurfa.2021.127145.

## Further reading

Penjumras, Patpen, et al., Russly B. Abdul Rahmana, Rosnita A. Talib, Khalina Abdan, 2014. Extraction and Characterization of Cellulose from Durian Rind. Agric. Agric. Sci. Procedia 2, 237–243. https://doi.org/10.1016/j.aaspro.2014.11.034.